Combined Primary Frequency Control Strategy of PMSG Based Wind Turbine

LIU Xiaoge[a], Zhao XU[a], Jian ZHAO[b]

[a] *The Department of Electrical Engineering, The Hong Kong Polytechnic University, Kowloon, Hong Kong SAR, People's Republic of China*

[b] *College of Electrical Engineering, Shanghai University of Electric Power, Shanghai, 200090, People's Republic of China*

E-mail: liuxiaoge07@gmail.com, eezhaoxu@polyu.edu.hk, zhaojianee@foxmail.com

Combined Primary Frequency Control Strategy of PMSG Based Wind Turbine

LIU Xiaoge[a], Zhao XU[a], Jian ZHAO[b]

[a] *The Department of Electrical Engineering, The Hong Kong Polytechnic University, Hong Kong SAR, China.*

[b] *College of Electrical Engineering, Shanghai University of Electric Power, Shanghai, 200090, China*

E-mail: liuxiaoge07@gmail.com, eezhaoxu@polyu.edu.hk, zhaojianee@foxmail.com

Abstract: To ensure the proper operation of power system, some independent system operators have specified that wind power plants should be able to participate in frequency control. This paper presents a combined control scheme exploiting the self-capability of PMSG based wind turbine to provide primary frequency response. In this scheme, the wind turbine operates in de-loading mode to obtain the power reserve under normal condition. On detecting frequency deviation, the proposed control strategy can not only utilize the power reserve and the kinetic energy of rotor for frequency regulation by adjusting the rotor speed, but employ the energy stored in DC capacitor to provide additional frequency support by slightly changing the DC-link voltage as well. The simulation results reveal that the wind turbines with the proposed method can improve frequency performance under both constant wind speed condition and variable wind speed condition.

Keywords: Permanent magnet synchronous generator (PMSG), wind turbine, primary frequency control, emulated inertia control, rotor speed control, DC-link voltage control

1 Introduction

Public concerns on climate change and energy crisis drive the increasing penetration of renewable energy sources into power grids. During the past decades, the integration of wind energy has experienced a sustainable growth [1]. It is expected that

more wind power plants (WPPs) will be installed in the immediate future. Traditionally, the maximum power point tracking (MPPT) control is implemented in variable speed wind turbines (VSWTs) to capture the maximum power from wind [2].

However, the growing wind power penetration actually imposes a great challenge on power system frequency stability, especially for isolated power grids [3], [4]. More specifically, owing to the application of power electronic devices, the rotor speed will not be coupled with system frequency [4]. If conventional power plants (CPPs) are progressively replaced by these VSWTs, the inertia of future power system will reduce significantly [3]. Apart from the reduction of system inertia, the variation of wind power can result in frequency fluctuation [5]. Therefore, to ensure the secure and stable operation of power system, the independent system operators (ISOs) in some European countries such as Ireland and UK, have published technical regulations and guidelines that require WPPs to participate in frequency control, especially when power demand is low [6].

So far, various frequency control schemes for individual wind turbine have been put forward. As discussed in [1] and [3], these approaches can be generally divided into two categories: the emulated inertia control (EIC) and the de-loading operation based primary frequency control (DOPFC). Both EIC and DOPFC can be applied in the rotor-side converter (RSC) control system of either doubly fed induction generator based wind turbine (DFIG-WT) or permanent magnet synchronous generator based wind turbine (PMSG-WT).

The EIC aims to provide virtual inertia support and thus improve the dynamic frequency performance [1]. A common method to provide the emulated inertia support is to extract the kinetic energy stored in rotor by applying the frequency derivative controller

[7-9]. Reference [7] advises that energy storage system (ESS) can be equipped for EIC. However, such method introduces additional hardware with extra costs [1].

DOPFC is usually applied in the wind turbines operating in de-loading mode. The VSWTs under de-loading operation can acquire power reserve because the extracted power from the wind is not maximized [3], [5], [10]. It is certainly inevitable that less power will be captured if the wind turbines are de-loaded. To compensate the revenue loss of WPPs' operators, the electricity market mechanism may be required to be modified [1], [11].

The objective of DOPFC is to utilize the reserve obtained from de-loading operation for frequency regulation. One method to implement DOPFC is to adjust the pitch angle [10-12]. The adjustment of pitch angle can lead to the regulation of captured mechanical power, but such control actions may cause mechanical fatigues [10]. Additionally, the participation of rotor for frequency control can be investigated further. Another method to achieve DOPFC is to add an active power compensation item, which is generated by frequency proportional controller, into the rotor-side converter control system of individual wind turbine [3], [5], [10], [13], [14]. However, the variation of mechanical power is not explicitly considered in these frequency control schemes. Consequently, the mechanical power captured from wind may not be regulated during the primary frequency control process [8], [12], [15].

During recent years, the PMSG-WTs have become more and more popular, especially for large wind farms [16]. Traditionally, the MPPT control is implemented by the rotor-side converter, while the grid-side converter (GSC) of PMSG-WT is set to stabilize the DC-link voltage [17]. Moreover, vector control technique with proportional-integral (PI) controllers or direct control technique with switching tables can be selected as

the inner loop control schemes of the converters [17-19]. In [20] and [21], a novel control scheme based on fractional-order controllers has been proposed. The two articles have shown that the power quality of the converters can be improved by using such control strategy.

For the PMSG-WT operating in de-loading mode, not only the power reserve and kinetic energy of rotor can be utilized for frequency control, but the energy stored in DC capacitor can be used to provide frequency support as well. The control schemes proposed in [1], [3], [5], [6], [8-14], [22] and [23] aim to employ the power reserve and kinetic energy stored in rotor for frequency control, but it seems that the usage of DC capacitor for frequency support is not discussed. The control strategies designed in [4], [7], [15], [16], [24] and [25] enable the PMSG-WTs to provide emulated inertia support, but the details about power reserve utilization for DOPFC have not been thoroughly investigated in these articles.

In order to make use of the power reserve acquired from de-loading operation, kinetic energy stored in rotor and the electrical energy in DC capacitor together for frequency control, we propose a combined primary frequency control strategy for PMSG-WT. A rotor speed adjusting control and a DC-link voltage regulating control are included in the proposed control scheme. Once frequency deviation is detected, both the rotor speed adjusting control and the DC-link regulating control will be activated simultaneously. With the rotor speed adjusting control, the rotor speed of each wind turbine can be varied according to frequency deviation. As a result, the mechanical power can be explicitly changed and thus power reserve acquired from de-loading operation can be used for frequency regulation. Meanwhile, due to the variation of the rotor speed, the kinetic energy

stored in the rotor can also be employed for realizing EIC. In addition, the DC-link voltage regulating control can utilize the energy in the DC capacitor for frequency support. Such controller can change the DC-link voltage so that additional EIC actions can be provided and thus the transient frequency performance can be improved further.

The rest of the paper is organized as follows: the PMSG-WT model for this study is described in Section II. Section III illustrates the proposed control scheme. Simulation results are provided in Section IV and conclusions are summarized in Section V.

2 Wind Turbine Model for Study

2.1 Overview of Conventional Control Scheme in Individual PMSG-WT

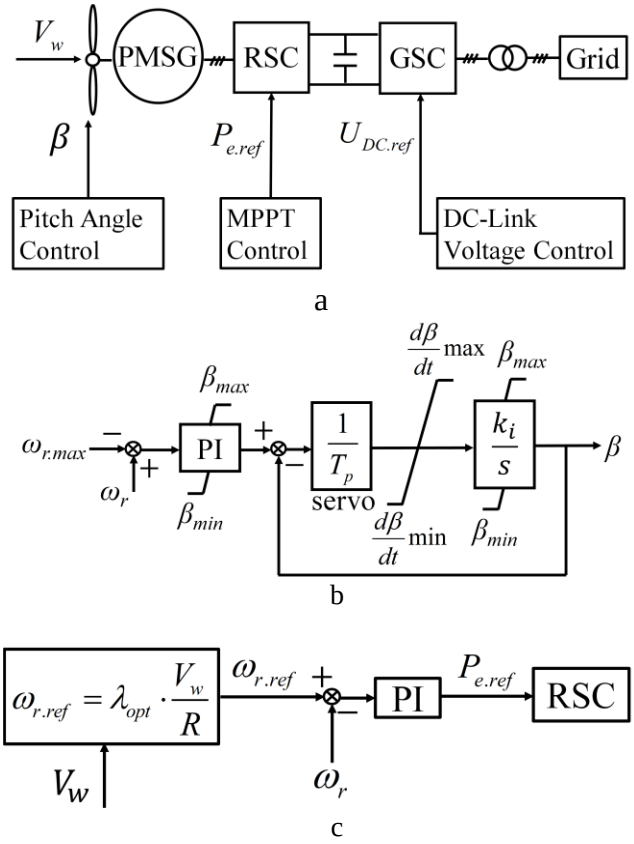

Figure. 1 Schematic diagram of a typical PMSG-WT

(a) overview of PMSG-WT control, (b) diagram of pitch angle controller, (c) typical MPPT control scheme

A typical model of individual 2 MW PMSG-WT described in [26] has been set up and the schematic diagram of the wind turbine is displayed in Figure. 1. The overview of the conventional control scheme in each PMSG-WT is described in Figure. 1(a) where $P_{e.ref}$ is the reference of active power obtained from MPPT control scheme and $U_{DC.ref}$ is the setting point of DC-link voltage.

In this model, the mechanical power P_m can be calculated as follows [26]:

$$P_m = 0.5C_p(\lambda,\beta)\rho\pi R^2 V_w^3 \tag{1}$$

$$C_p = 0.5176(\frac{116}{\gamma} - 0.4\beta - 5)e^{-\frac{21}{\gamma}} + 0.0068\lambda \tag{2}$$

$$\gamma = 1/(\frac{1}{\lambda + 0.08\beta} - \frac{0.035}{\beta^3 + 1}) \tag{3}$$

where C_p is power coefficient; λ is tip speed ratio (TSR); β is pitch angle; ρ is air density; R is the radius of the blade; V_w is wind speed.

2.2 Model of Drive Train

To describe the dynamic performance of drive train, it is necessary to adopt a two-mass model [27]. Such model can be expressed by the following equations:

$$T_m = \frac{0.5\rho\pi R^2 C_p(\lambda,\beta)V_W^3}{\omega_t} \tag{4}$$

$$\frac{d\omega_t}{dt} = \frac{1}{2H_t}(T_m - T_{sh}) \tag{5}$$

$$\frac{d\theta_t}{dt} = \omega_b(\omega_t - \omega_r) \tag{6}$$

$$\frac{d\omega_r}{dt} = \frac{1}{2H_g}(T_{sh} - T_e - B\omega_r) \tag{7}$$

$$T_{sh} = K_{sh}\theta_t + D_{sh}\omega_b(\omega_t - \omega_r) \tag{8}$$

where T_m is mechanical torque, ω_t is the speed of wind turbine; T_{sh} is shaft torque; H_t is turbine inertia constant; θ_t is shaft twist angle, ω_b is the base value of rotating speed; ω_r

is rotor speed, H_g is the inertia constant of generator, B is the friction coefficient of the generator, K_{sh} is the constant of stiffness and D_{sh} is mutual damping.

2.3 Model of Pitch Controller

The pitch angle controller is used to protect the wind turbine from over-speeding if the wind speed is too high. Usually, the pitch angle β is set as its optimal value β_{opt}. A common value of β_{opt} is zero [28]. If the wind speed is so high that rotor speed exceeds the upper bound $\omega_{r.max}$, the pitch angle controller will be triggered to limit the rotating speed. The pitch angle control system described in [27] is used in this paper. The model of the pitch angle actuator is presented in Figure. 1(b) where T_p and k_i are the parameters of the system.

2.4 Conventional Control Schemes in Rotor-Side Converter and Grid-Side Converter

Conventionally, the rotor-side converter in each PMSG-WT is arranged to implement the MPPT control, so the wind turbine can be driven to the optimal speed where the maximum power can be captured. In [2], a typical MPPT with a rotor speed control loop is proposed. Figure. 1(c) presents such MPPT controller, where $\omega_{r.ref}$ is the reference of rotor speed. λ_{opt} is the TSR where the extracted power is optimal. $P_{e.ref}$ is the active power reference produced by PI controller. Besides, Figure. 1(a) shows that the DC-link voltage control is performed by grid-side converter. Under normal condition, the DC-link voltage should be kept constant and thus the active power generated by RSC can be delivered to the power grid. Therefore, the DC-link voltage controller with constant $U_{DC.ref}$ is adopted in GSC. In this paper, the modelling of the converters is based on the description in [17].

According to the grid codes published by ISOs, the WPPs should satisfy the requirements of power quality. The power quality issues are associated with the topology of converter and the control technique used in the converters. In this paper, we focus on the development of frequency control scheme. The power quality issues are beyond the scope of this research.

3 The Proposed Primary Frequency Control Scheme for PMSG-WT

3.1 Overview of Proposed Control Scheme

Under normal condition, the PMSG-WTs can obtain the primary reserve if the wind turbine rotates at a certain speed where the extracted power is not optimal. In this paper, the de-loading operation is realized by using over-speeding technique so that additional kinetic energy can be stored for frequency control. The theoretical analysis and the implementation scheme of over-speeding based de-loading operation are provided in Section 3.2.

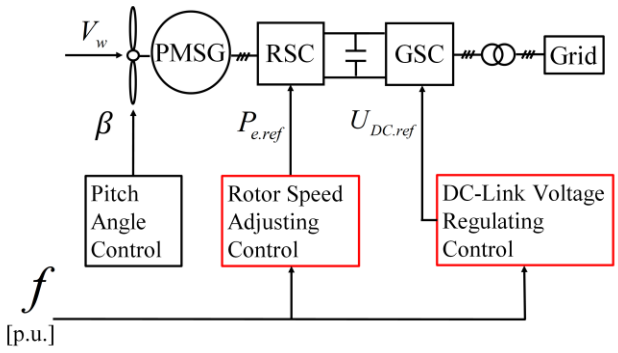

Figure. 2 Overview of proposed frequency control scheme

To take part in frequency regulation, the power reserve acquired from de-loading operation should be used. Hence, a rotor speed adjusting control is applied herein. If such control scheme is utilized, the fall of system frequency can result in the reduction of rotor speed reference. Therefore, the rotor speed of each wind turbine will start to decrease and

evolve towards to the MPPT point. In this process, not only the kinetic energy stored in rotor can be released to the power system, but more power can be captured and injected to the power grid as well. The wind turbine will eventually operate at a new speed where more power can be harvested. On the contrary, the rise of system frequency can cause the wind turbine to accelerate so that more kinetic energy can be stored and less power can be extracted.

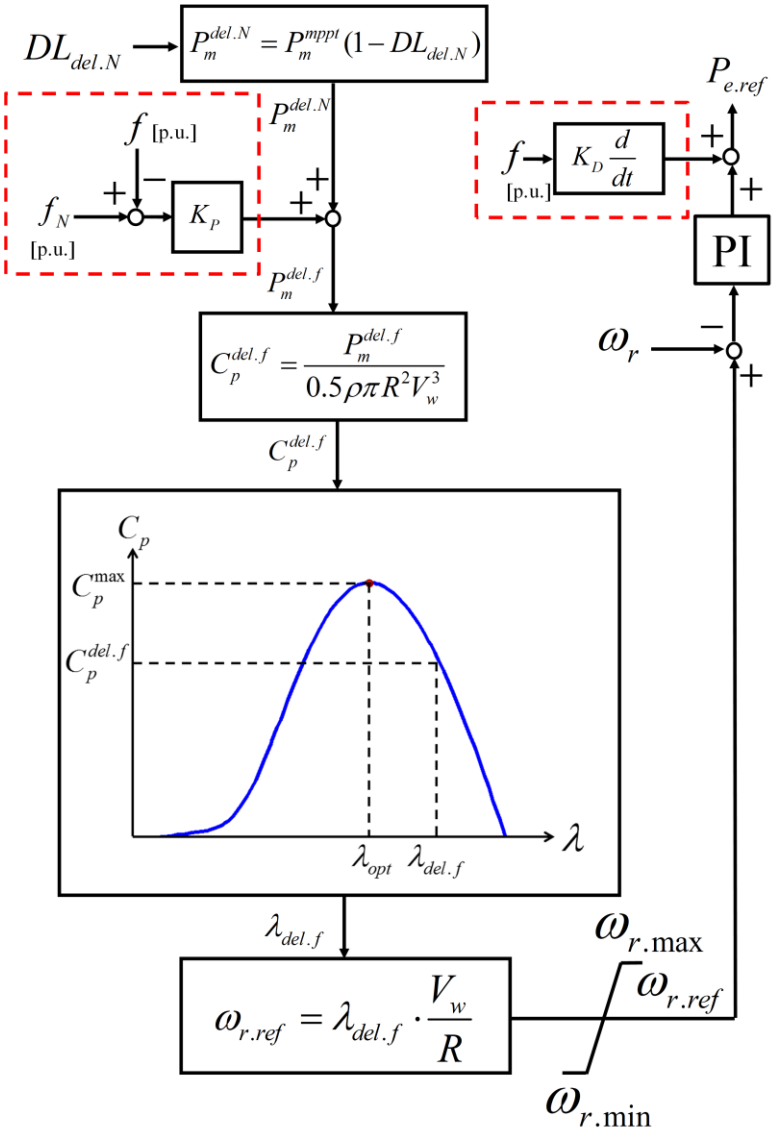

a

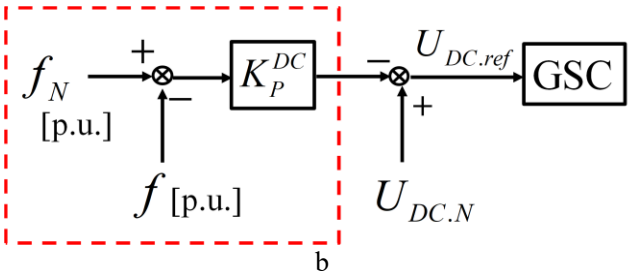

Figure. 3 Proposed frequency control scheme

(a) rotor speed adjusting control (b) DC-link voltage regulating control

Besides, a DC-link voltage regulating control is applied to utilize the energy stored in DC capacitor for emulated inertia support. If frequency deviates, the DC capacitor with the new controller will absorb or release energy by continuously adjusting the value of DC-link voltage. Consequently, the DC capacitor can contribute to the dynamic frequency response.

The combined primary frequency control scheme of PMSG-WT can be summarized as Figure. 2 depicts. The rotor speed adjusting control scheme which is applied in RSC control system is shown in Figure. 3(a). Figure. 3(b) shows the DC-link voltage regulating control. The details of the proposed control strategy have been illustrated in Section. 3.3 and 3.4.

3.2 De-loading Operation of PMSG-WT Under Normal Condition

According to the discussion in [29], the de-loading level under normal condition $DL_{del.N}$ of each wind turbine can be defined as (9):

$$\begin{aligned} DL_{del.N} &= \frac{P_m^{mppt} - P_m^{del.N}}{P_m^{mppt}} \times 100\% \\ &= \frac{0.5C_p^{\max}\rho\pi R^2 V_W^3 - 0.5C_p^{del.N}\rho\pi R^2 V_W^3}{0.5C_p^{\max}\rho\pi R^2 V_W^3} \times 100\% \\ &= \frac{C_p^{\max} - C_p^{del.N}}{C_p^{\max}} \times 100\% \end{aligned} \tag{9}$$

where P_m^{mppt} is the maximum power for a given wind speed and $P_m^{del.N}$ is the captured power under de-loading operation. C_P^{max} is the maximum value of power coefficient. $C_P^{del.N}$ is a sub-optimal power coefficient. For a given $DL_{del.N}$, the corresponding power $P_m^{del.N}$ can be derived from (10):

$$P_m^{del.N} = P_m^{mppt}(1 - DL_{del.N}) \tag{10}$$

To achieve a certain de-loading level, the rotor speed of the wind turbine should shift from its optimal value determined by λ_{opt} [5]. If the pitch angle is set as β_{opt}, the relationship between λ and power coefficient C_p can be described as Figure. 4(a) shows.

Figure. 4(a) shows that both a lower-than-optimal TSR $\lambda'_{del.N}$ and a higher-than-optimal TSR $\lambda_{del.N}$ can be used to acquire a given $DL_{del.N}$ [30]. $\lambda'_{del.N}$ indicates that de-loading operation can be realized by under-speeding, while the $\lambda_{del.N}$ reveals that $C_P^{del.N}$ can be achieved by over-speeding [5], [30]. It is preferable to use over-speeding technique for de-loading operation realization, because the additional kinetic energy can be stored by accelerating [23].

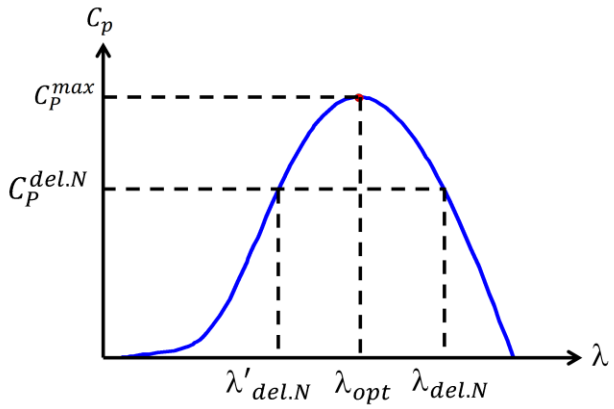

a

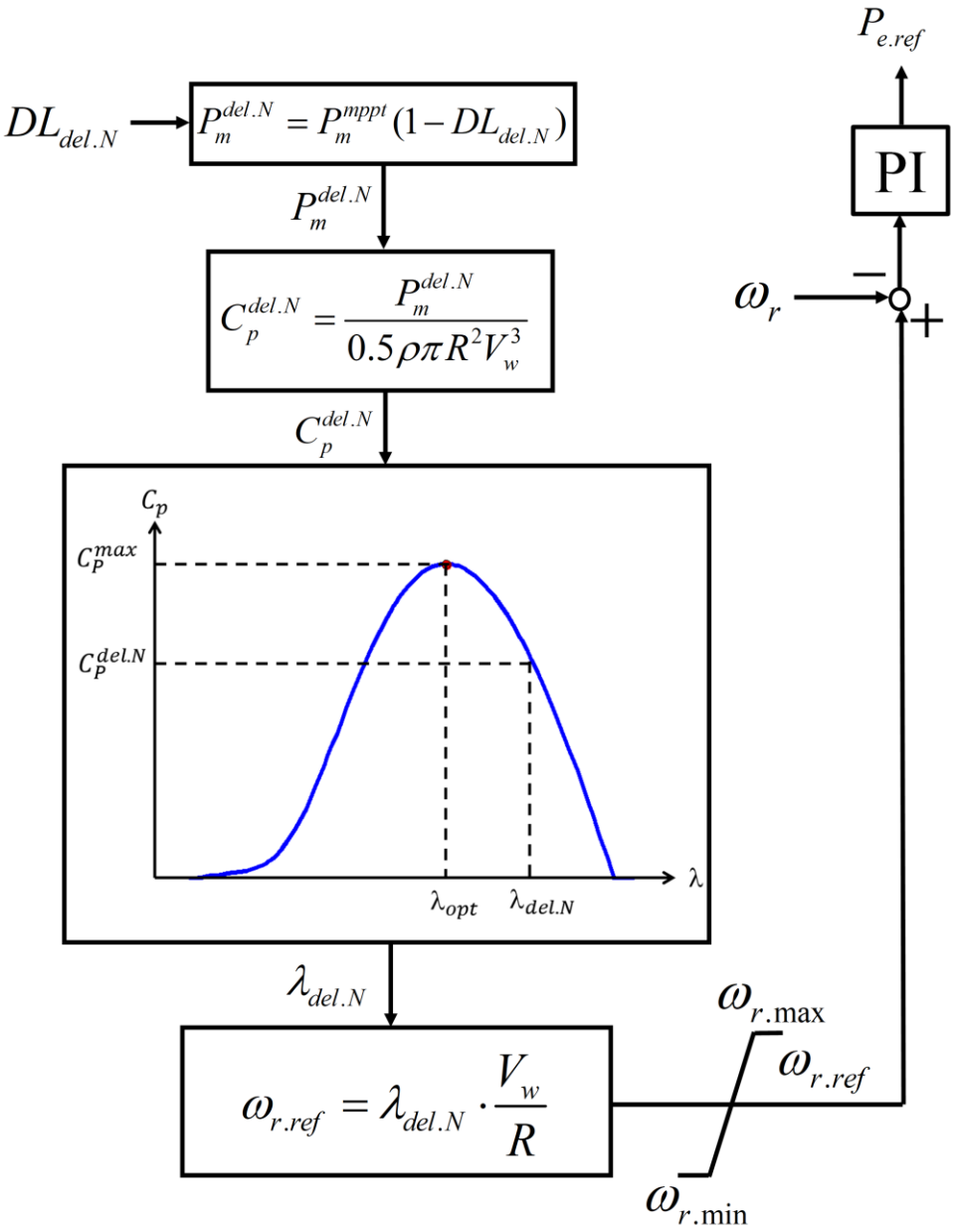

b

Figure. 4 De-loading operation of individual PMSG-WT

(a) $C_P - \lambda$ characteristics (b) control scheme to realize de-loading operation

In order to implement the over-speeding based de-loading operation, the MPPT control in RSC should be replaced by the control scheme presented in Figure. 4(b) where $\omega_{r.min}$ is the lower limit of rotor speed. As shown in Figure. 4(b), the value of $C_P^{del.N}$ can be given by using (1). Subsequently, the corresponding TSR $\lambda_{del.N}$ which is higher than

λ_{opt} can be obtained from the $C_P - \lambda$ characteristics.

It should be noted that the over-speeding technique discussed in this paper can be applied only if the wind speed is not very high and the pitch angle control is not activated. If wind speed is great enough and rotor speed reaches the maximum value, the pitch angle controller will be triggered. In that case, the de-loading operation can be achieved by coordinating rotor speed control with pitch angle control [10], [22], [23]. Such control scheme will be investigated further in the future. In addition, the implementation of such control method relies on the accuracy of wind speed measurement. As mentioned in [31], the light detection and ranging system (LIDAR) can be regarded as a promising technique to obtain wind speed information for the application of wind turbine control schemes.

3.3 Rotor Speed Adjusting Control for Frequency Response

As mentioned in Section 3.1, for frequency regulation, more power should be captured from wind when frequency drops, while the extracted power is required to decrease in the event of over-frequency incident. Such requirements can be fulfilled if the reference of rotor speed is generated as Figure. 3(a) shows.

In Figure. 3(a), f_N is the nominal value of frequency and f is the system frequency measured in real-time. $P_m^{del.f}$ denotes the desirable value of mechanical power in case of frequency deviation. The value of $P_m^{del.f}$ is acquired by adding the $P_m^{del.N}$ to the compensating item produced by the frequency proportional (P) controller. The K_P in the P controller is the parameter. The method to determine K_P is provided in Section IV. According to (1) and the $C_P - \lambda$ characteristics, the power coefficient and the TSR under frequency excursions, which are represented by $C_P^{del.f}$ and $\lambda_{del.f}$ respectively, can be obtained if $P_m^{del.f}$ is given. The $\lambda_{del.f}$ can be used to update the reference of rotor speed

$\omega_{r.ref}$ so that the wind turbine can be driven to the new operating point.

According to the wind turbine characteristics, the power reference $P_m^{del.f}$ can be used to generate the reference of rotor speed $\omega_{r.ref}$. Such rotor speed reference can be sent to the PI speed controller so that the operating point of the wind turbine can be manipulated for frequency support. By using such control scheme, the wind turbine will approach to the MPPT point and more mechanical power can be captured when frequency dips. Therefore, additional active power can be produced for primary frequency support. In case of over-frequency event, the wind turbine can move towards a new operating point where less power is extracted.

Different from the rotor speed control scheme discussed in [22], a frequency derivative compensation item with the parameter K_D is added in the control scheme shown in Figure.3(a) for a trivial improvement. Because of the rotor speed adjustment, the D controller can utilize the kinetic energy to perform EIC so that the dynamic frequency behavior can be improved. Additionally, the drive train system is described by two-mass model in this research. In fact, the shaft stiffness K_{sh} of the model is small and the connection between the turbine and generator is relatively soft [27]. Consequently, torsion oscillation can be observed and such oscillation can lead to frequency fluctuation [27]. The frequency derivative controller can also help to suppress the fluctuating behavior of the frequency caused by torsion oscillation.

3.4 DC-link Voltage Regulating Control for Frequency Response

Under normal condition, the DC-link voltage in the PMSG-WT should be kept constant. As investigated in [25] and [32], the energy stored in the DC capacitor can be utilized to provide additional emulated inertia support so that the dynamic performance of

frequency can be improved further. The additional EIC function can be realized if the power P_e^{DC}, which is provided by DC capacitor, is generated by frequency derivative controller and thus the following equation can be acquired:

$$P_e^{DC} = U_{DC} \cdot C_{DC} \frac{dU_{DC}}{dt} = K_D^{DC} \cdot \frac{df}{dt} \tag{11}$$

where K_D^{DC} is the parameter.

According to the principles of integration, the energy released by DC capacitor can be derived as [24], [32]:

$$\int_{t_0}^{t} P_e^{DC} \cdot dt = \int_{U_{DC.N}}^{U_{DC}} U_{DC} \cdot C_{DC} \cdot dU_{DC} = \int_{f_N}^{f} K_D^{DC} \cdot f \cdot df \tag{12}$$

where t_0 is the instant when frequency begins to deviate, $U_{DC.N}$ is the nominal value of DC-link voltage under normal condition, while U_{DC} is the actual value. C_{DC} represents the capacitance. Therefore, we can obtain that:

$$\frac{1}{2} C_{DC} \left(U_{DC}^2 - U_{DC.N}^2 \right) = \frac{1}{2} K_D^{DC} (f^2 - f_N^2) \tag{13}$$

$$\frac{1}{2} C_{DC} \left[\left(U_{DC.N} + \Delta U_{DC} \right)^2 - U_{DC.N}^2 \right] = \frac{1}{2} K_D^{DC} \left[\left(f_N + \Delta f \right)^2 - f_N^2 \right] \tag{14}$$

where ΔU_{DC} is the variation of DC-link voltage and the Δf denotes the variation of system frequency. Considering that both ΔU_{DC} and Δf can be relatively small, the higher order terms ΔU_{DC}^2 and Δf^2 in (14) can be neglected and the equation can be simplified as (15) or (16) [24]:

$$C_{DC} \cdot U_{DC.N} \cdot \Delta U_{DC} = K_D^{DC} \cdot f_N \cdot \Delta f \tag{15}$$

$$C_{DC} \cdot U_{DC.N} \cdot \left(U_{DC} - U_{DC.N} \right) = K_D^{DC} \cdot f_N \cdot (f - f_N) \tag{16}$$

Equation (16) illustrates that the voltage of DC capacitor U_{DC} can be varied with

system frequency f so that the emulated inertia support can be provided. Furthermore, the U_{DC} can be expressed as:

$$U_{DC} = -K_P^{DC} \cdot (f_N - f) + U_{DC.N} \tag{17}$$

where K_P^{DC} is also a parameter and the value can be computed by:

$$K_P^{DC} = \frac{K_D^{DC} \cdot f_N}{C_{DC} \cdot U_{DC.N}} \tag{18}$$

According to (11)~(17), it can be concluded that the emulated inertia support can be provided if the $U_{DC.ref}$ is given as Figure. 3(b) displays.

By using the controller shown in Figure. 3(b), the DC-link voltage should reduce so that the energy can be provided when frequency drops. If frequency rises, the voltage of DC capacitor should increase actively to store more energy. The value of K_P^{DC} can affect the range of DC-link voltage variation and the determination of K_P^{DC} is conducted in Section IV.

As mentioned in Section II, the power quality issues of the wind power plant should be considered in practice. According to the investigation in [33-35], the power quality of each wind turbine can be improved by using several methods, such as installing LCL filter or implementing repetitive control techniques. Further discussion on power quality will be carried out in the immediate future.

4 Simulation Results

As presented in Figure. 5, a small power system model is constructed. The system consists of 5 wind turbines and 2 thermal power plants (TPPs). The system model is built up in Matlab/Simulink. The nominal value of the system frequency is set as 50Hz. The parameters of the governors in the thermal power plants can be found in [36]. The total

capacity of all the power plants is 85 MVA and thus the capacity level of wind energy is 11.76%. According to the data listed in [37], the damping coefficient of load is set as 1.5 herein. The initial load is set as (39.567+j2.7067) MVA. The other parameters of the system can be found in Appendix.

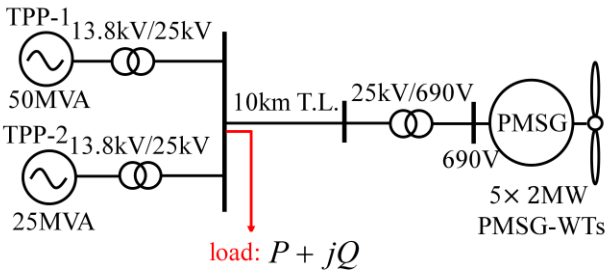

Figure.5 Power system model

To validate the effectiveness of the proposed control scheme, the following control strategies are used for comparison:

***Strategy A*:** The PMSG-WT operates in MPPT mode and no frequency control is implemented.

***Strategy B*:** The rotor speed adjusting control is applied alone in the wind turbine, while the DC-link voltage regulating control is not used.

***Strategy C*:** Both the rotor speed adjusting control and DC-link voltage regulating control are utilized.

In this research, the method to calculate the value of K_P in Figure. 3(a) is given by (19):

$$K_P = \frac{P_m^{mppt} - P_m^{del.N}}{f_N - f_{min}^{WT}} \times f_N \tag{19}$$

where f_{min}^{WT} is the lower limit of control range, i.e. when the system frequency decreases to f_{min}^{WT}, the PMSG-WT will return to the MPPT operating point and all the primary reserve

will be released. The K_P calculated by (19) is also applied in the proposed control scheme if over-frequency events occur. From (19), we can learn that the wind turbine can be more sensitive to the frequency deviation if f_{min}^{WT} is greater.

For simplicity of the test, if Strategy B or Strategy C is used, the de-loading level of each wind turbine under normal condition is kept as 10% and f_{min}^{WT} is set as 49.8 Hz. In this paper, we focus on how to utilize the reserve acquired from the wind turbines with a certain de-loading level for frequency response. Therefore, the study of $DL_{del.N}$ determination can be carried out in the future.

Moreover, the parameter of the DC-link voltage regulating control K_P^{DC} is calculated by (20), where $U_{DC.min}$ denotes the minimum value of DC-link voltage. In this research, $U_{DC.min}$ is set as 0.85p.u.. The maximum voltage of DC-link $U_{DC.max}$ is set as 1.15 p.u.. From (20), it can be learned that if the frequency increases to 50.2 Hz, the maximum value of DC-link voltage will be achieved.

$$K_P^{DC} = \frac{U_{DC.N} - U_{DC.\min}}{f_N - f_{\min}^{WT}} \times f_N \tag{20}$$

The selection of these parameters, which aims at optimizing the performance of the proposed control scheme, will be investigated in the future as well. In addition, the impact of C_{DC} on frequency behavior is analyzed in Section 4.4.

The maximum absolute value of the rate of change of frequency, which is denoted by maximum $|ROCOF|$, frequency nadir f_{nadir} and the final value of frequency during the simulated process f_{final} are used to evaluate the primary frequency control performance under constant wind speed. It is noteworthy that in this paper, the f_{nadir} is defined as the frequency value measured when the maximum dynamic frequency deviation is achieved.

Furthermore, if an under-frequency event occurs, the f_{nadir} is the lowest value of frequency, while when frequency rises, the f_{nadir} is the peak value of frequency.

The maximum $|ROCOF|$ and f_{nadir} can represent the dynamic frequency performance and f_{final} can roughly describe the steady-state behavior. Besides, the mean value of absolute value of system frequency variation, which is denoted by mean value of $|\Delta f|$, and f_{nadir} is applied to assess the frequency performance under variable wind speed.

4.1 Sudden Load Increase Under Constant Wind Speed

Case. A: Wind speed is set as 8m/s and load increases by (7.5+j0.75) MVA at 40s.

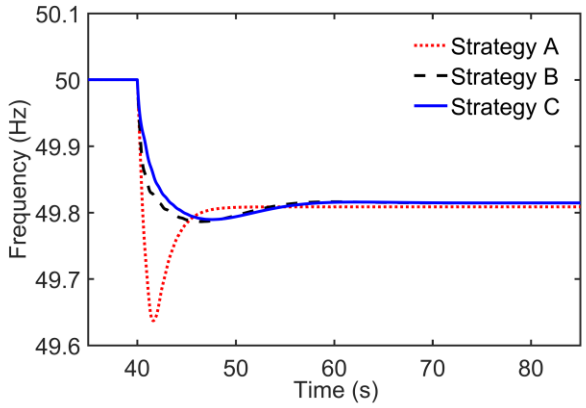

a

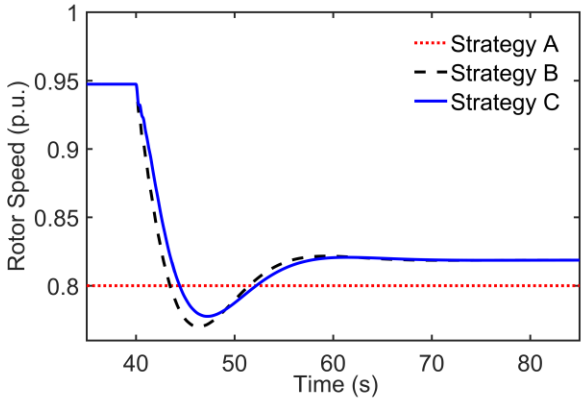

b

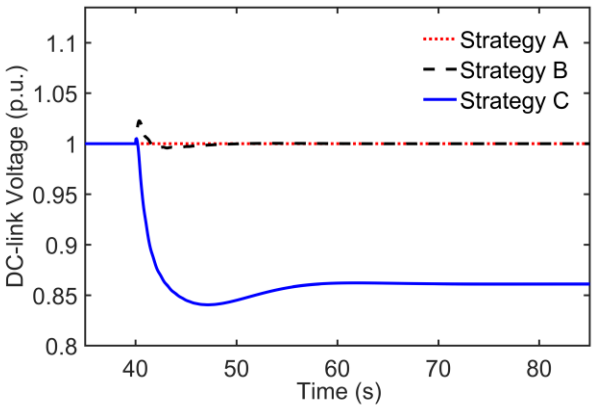

c

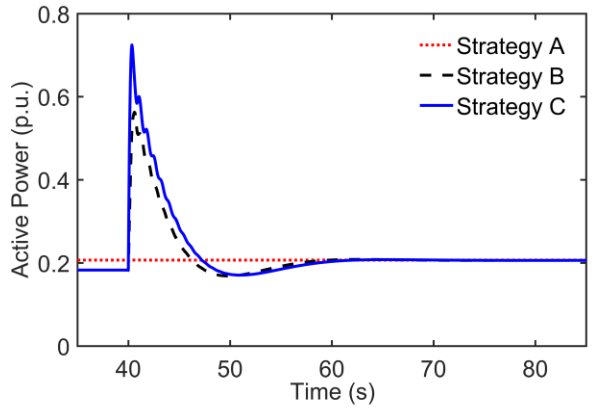

d

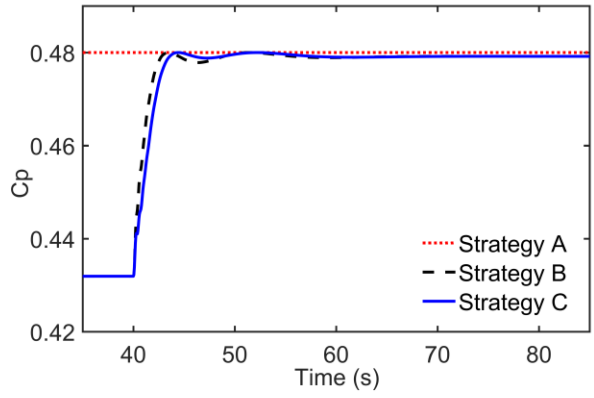

e

Figure. 6 Simulation results of Case. A

(a) variation of system frequency in Case. A, (b) variation of rotor speed in Case. A, (c) variation of DC-link voltage in Case. A, (d) variation of active power produced by each PMSG-WT in Case. A, (e) variation of power coefficient C_p in Case. A

Table 1 Frequency performance of Case. A

Schemes	Maximum |ROCOF| (Hz/s)	f_{nadir} (Hz)	f_{final} (Hz)
Strategy A	0.3884	49.6372	49.8087
Strategy B	0.3268	49.7864	49.8146
Strategy C	0.2988	49.7895	49.8146

Figure. 6 presents the simulation results of Case. A. The data describing frequency behavior are listed in Table 1. The data in Table 2-Table 5 show the performance of wind turbines and thermal power plants. Because the over-speeding technique is adopted, the rotor speed for de-loading operation (0.9473 p.u.) is higher than the optimal value (0.8 p.u.) in this case.

Table 2 reveals that the wind turbine with Strategy A cannot react to the frequency event and the rotor speed remains at 0.8 p.u., while the rotor speed of PMSG-WT can reduce from 0.9473 p.u. to 0.8187 p.u. by using Strategy B or Strategy C. As a result, the kinetic energy in rotor can be released and mechanical power increases from 0.1946 p.u. to 0.2159 p.u.. Therefore, the maximum $|ROCOF|$ decreases significantly, while the f_{nadir} is improved greatly. Besides, f_{final} can increase from 49.8087 Hz to 49.8146 Hz.

Moreover, Figure. 6(c) shows that the DC-link voltage will decrease when Strategy C is used. Therefore, the energy stored in DC capacitor is delivered to the power grid and more frequency support is provided. Hence, compared to the performance of Strategy B, maximum $|ROCOF|$ reduces from 0.3268 Hz/s to 0.2988 Hz/s and f_{nadir} improves from 49.7864 Hz to 49.7895 Hz. It should be noted that the DC capacitor can only provide

temporary active power support and thus the value of f_{final} will not be influenced.

Table 2 Wind turbine performance of Case. A

Schemes	Initial Value of ω_r (p.u.)	Final Value of ω_r (p.u.)	Initial Value of P_m(p.u.)	Final Value of P_m (p.u.)
Strategy A	0.8	0.8	0.2163	0.2163
Strategy B	0.9473	0.8187	0.1946	0.2159
Strategy C	0.9473	0.8187	0.1946	0.2159

Table 3 States of each PMSG-WT in Case. A

Schemes	Initial Active Power (p.u.)	Final Active Power (p.u.)	Initial Reactive Power (p.u.)	Final Reactive Power (p.u.)
Strategy A	0.2067	0.2067	0	0
Strategy B	0.1826	0.2061	0	0
Strategy C	0.1826	0.2061	0	0

Table 4 States of 50MVA Thermal Power Plant in Case.A

Schemes	Initial Active Power (p.u.)	Final Active Power (p.u.)	Initial Reactive Power (p.u.)	Final Reactive Power (p.u.)
Strategy A	0.5150	0.6046	0.0527	0.0755
Strategy B	0.5197	0.6089	0.0529	0.0769
Strategy C	0.5197	0.6080	0.0529	0.0772

Table 5 States of 25MVA Thermal Power Plant in Case. A

Schemes	Initial Active Power (p.u.)	Final Active Power (p.u.)	Initial Reactive Power (p.u.)	Final Reactive Power (p.u.)
Strategy A	0.5188	0.6084	0.0508	0.0686
Strategy B	0.5187	0.6081	0.0509	0.0700
Strategy C	0.5187	0.6072	0.0509	0.0704

4.2 Sudden Load Decrease Under Constant Wind Speed

Case. B: Wind speed is set as 8m/s and load decreases by (7.5+j0.75) MVA at 40s

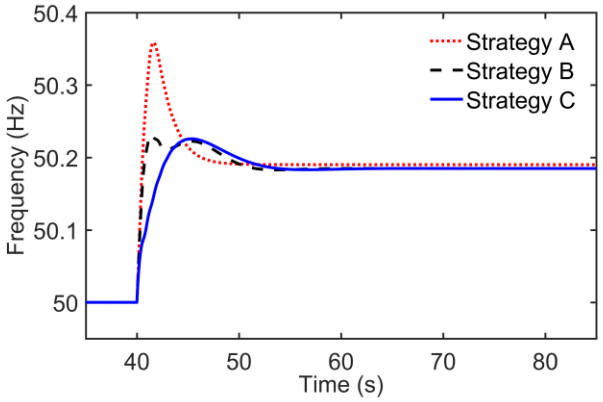
Strategy A
Strategy B
Strategy C
Frequency (Hz)
50.4
50.3
50.2
50.1
50
40
50
60
70
80
Time (s)

a

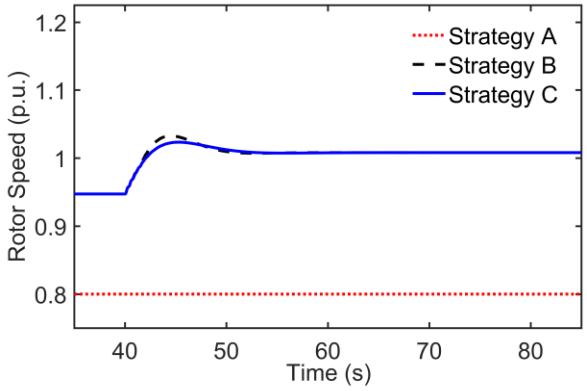
Strategy A
Strategy B
Strategy C
Rotor Speed (p.u.)
1.2
1.1
1
0.9
0.8
40
50
60
70
80
Time (s)

b

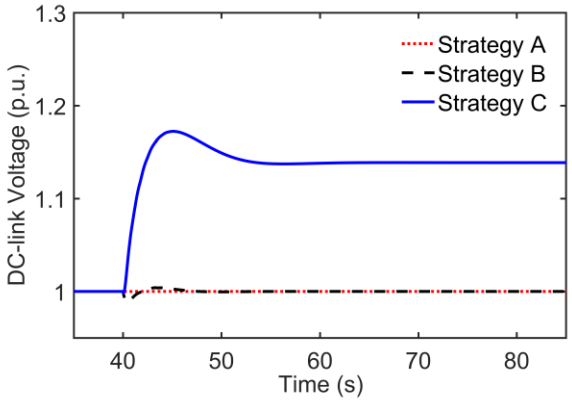
Strategy A
Strategy B
Strategy C
DC-link Voltage (p.u.)
1.3
1.2
1.1
1
40
50
60
70
80
Time (s)

c

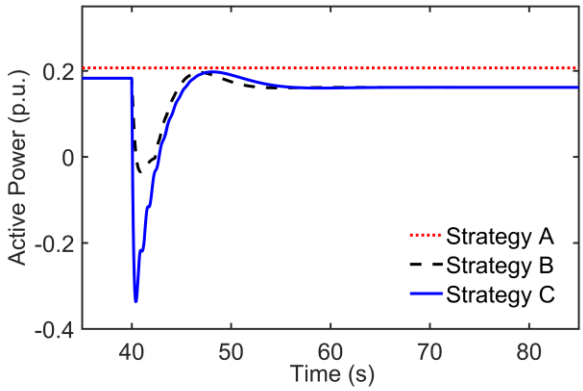

d

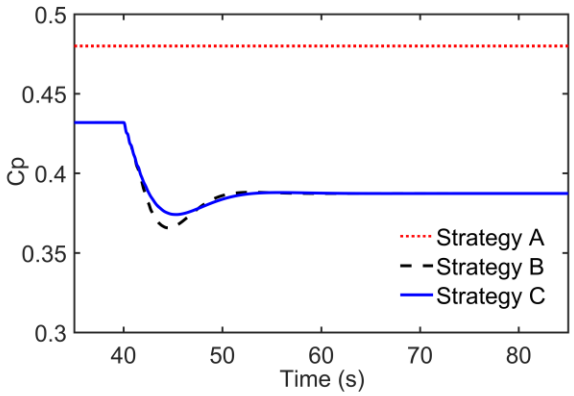

e

Figure. 7 Simulation results of Case. B

(a) variation of system frequency in Case. B, (b) variation of rotor speed in Case. B, (c) variation of DC-link voltage in Case. B, (d) variation of active power produced by each PMSG-WT in Case. B, (e) variation of power coefficient C_p in Case. B

As displayed in Figure. 7 and Table 6, the wind turbines with Strategy A can lead to the greatest overshoot, because no frequency response is provided. However, by using Strategy B or Strategy C, the wind turbine accelerates and move towards to a new operating point where less power is captured. The increment of rotor speed indicates that the additional power in the power grid can be stored so that the power imbalance can be

mitigated. In addition, due to the reduction of power production, the value of f_{final} decreases from 50.1901 Hz to 50.1849 Hz.

Table 6 Frequency response of Case. B

Schemes	Maximum |ROCOF|(Hz/s)	f_{nadir} (Hz)	f_{final} (Hz)
Strategy A	0.3822	50.3587	50.1901
Strategy B	0.3397	50.2310	50.1849
Strategy C	0.3087	50.2259	50.1849

Table 7 Wind turbine performance of Case. B

Schemes	Initial Value of ω_r (p.u.)	Final Value of ω_r (p.u.)	Initial Value of P_m (p.u.)	Final Value of P_m (p.u.)
Strategy A	0.8	0.8	0.2163	0.2163
Strategy B	0.9473	1.0080	0.1946	0.1745
Strategy C	0.9473	1.0080	0.1946	0.1745

Table 8 States of each PMSG-WT in Case. B

Schemes	Initial Active Power (p.u.)	Final Active Power (p.u.)	Initial Reactive Power (p.u.)	Final Reactive Power (p.u.)
Strategy A	0.2067	0.2067	0	0
Strategy B	0.1826	0.1614	0	0
Strategy C	0.1826	0.1614	0	0

Table 9 States of 50MVA Thermal Power Plant in Case. B

Schemes	Initial Active Power (p.u.)	Final Active Power (p.u.)	Initial Reactive Power (p.u.)	Final Reactive Power (p.u.)
Strategy A	0.5150	0.4200	0.0527	0.0380
Strategy B	0.5197	0.4266	0.0529	0.0354
Strategy C	0.5197	0.4257	0.0529	0.0362

Table 10 States of 25MVA Thermal Power Plant in Case. B

Schemes	Initial Active Power (p.u.)	Final Active Power (p.u.)	Initial Reactive Power (p.u.)	Final Reactive Power (p.u.)
Strategy A	0.5188	0.4239	0.0508	0.0413
Strategy B	0.5187	0.4255	0.0509	0.0386
Strategy C	0.5187	0.4246	0.0509	0.0395

Figure. 7 also verifies that the DC-link voltage regulating controller can boost the voltage of DC capacitor after being subjected to the over-frequency event. The increment of DC-link voltage suggests that the additional active power can be absorbed by the DC capacitor as well, so the maximum $|ROCOF|$ decreases to 0.3087 Hz/s and f_{nadir} reduces to 50.2259 Hz.

4.3 Sudden Load Increase Under Variable Wind Speed

Case. C Wind speed is variable and load increases by (7.5+*j*0.75) MVA at 180s

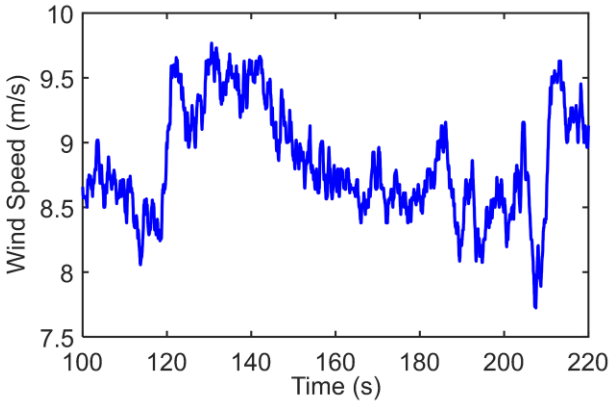

Figure. 8 Variable wind speed profile for Case. C

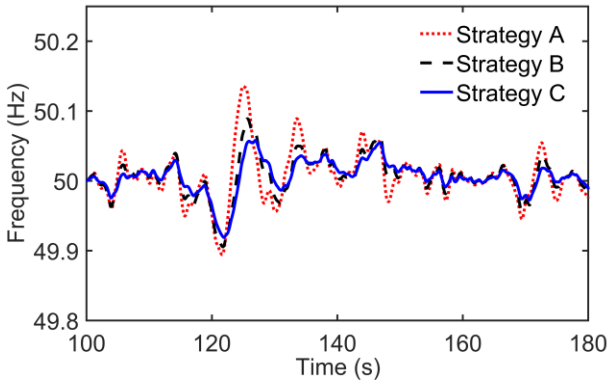

a

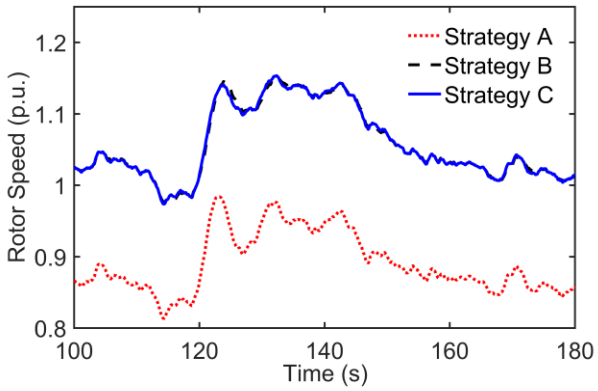
Strategy A
Strategy B
Strategy C
Rotor Speed (p.u.)
1.2
1.1
1
0.9
0.8
100
120
140
160
180
Time (s)

b

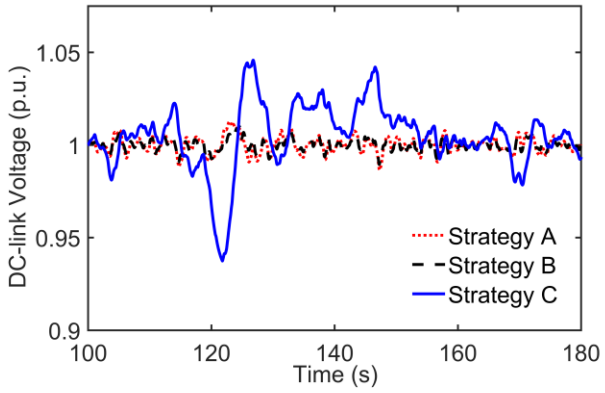
DC-link Voltage (p.u.)
1.05
1
0.95
0.9
Strategy A
Strategy B
Strategy C
100
120
140
160
180
Time (s)

c

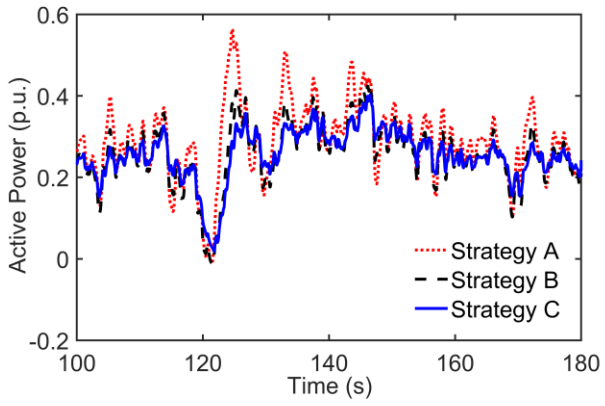
Active Power (p.u.)
0.6
0.4
0.2
0
-0.2
Strategy A
Strategy B
Strategy C
100
120
140
160
180
Time (s)

d

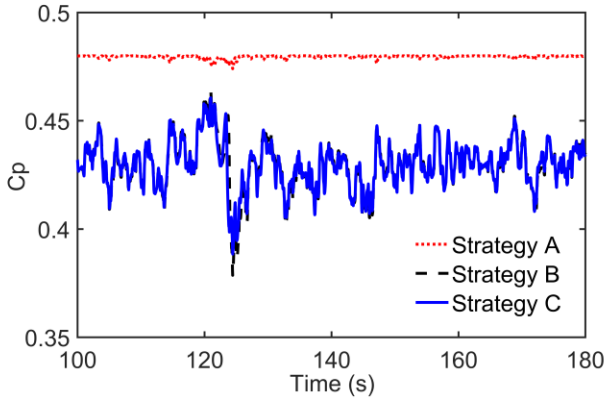

e

Figure. 9 Simulation results of Case. C (100s~180s)

(a) variation of system frequency in Case. C (100s~180s), (b) variation of rotor speed in Case. C (100s~180s), (c) variation of DC-link voltage in Case. C (100s~180s), (d) variation of active power produced by each PMSG-WT in Case. C (100s~180s), (e) variation of power coefficient C_p in Case. C (100s~180s)

The variable wind speed profile for Case. C is provided in Figure. 8. The data of wind speed is downloaded from [38]. In this case, load remains constant during 100s~180s.

Figure. 9 describes the simulation results during 100s~180s. Table 11 provides the data in this period. From the results, we can learn that the varied wind speed can cause the system frequency to fluctuate, but both Strategy B and Strategy C can help to suppress the frequency fluctuation because the rotor speed adjusting control is applied and thus operating point of each PMSG-WT can be changed according to frequency deviation. The results also prove that the application of Strategy C can result in the smallest mean value of $|\Delta f|$ as well as the smoothest frequency curve, as the DC capacitor is also arranged to provide frequency response.

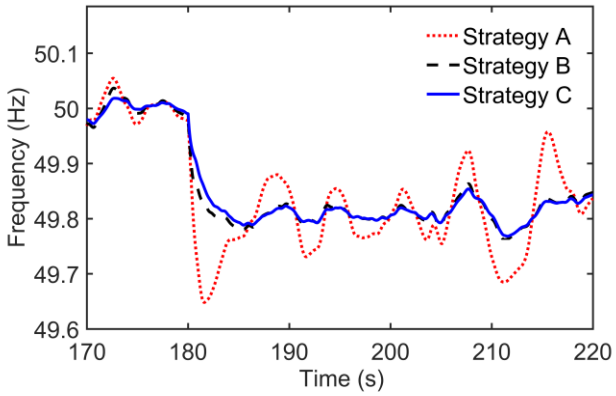
Strategy A
Strategy B
Strategy C
Frequency (Hz)
50.1
50
49.9
49.8
49.7
49.6
170
180
190
200
210
220
Time (s)

a

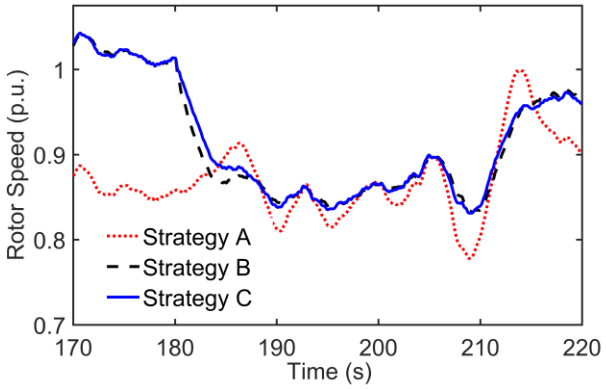
Rotor Speed (p.u.)
1
0.9
0.8
0.7
Strategy A
Strategy B
Strategy C
170
180
190
200
210
220
Time (s)

b

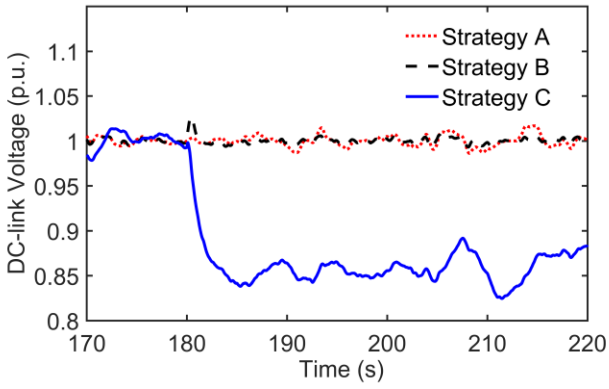
DC-link Voltage (p.u.)
1.1
1.05
1
0.95
0.9
0.85
0.8
Strategy A
Strategy B
Strategy C
170
180
190
200
210
220
Time (s)

c

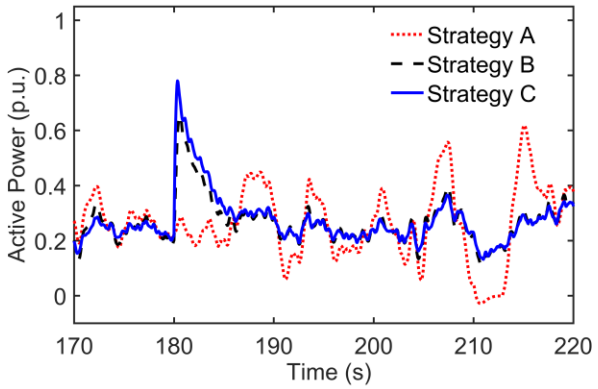

d

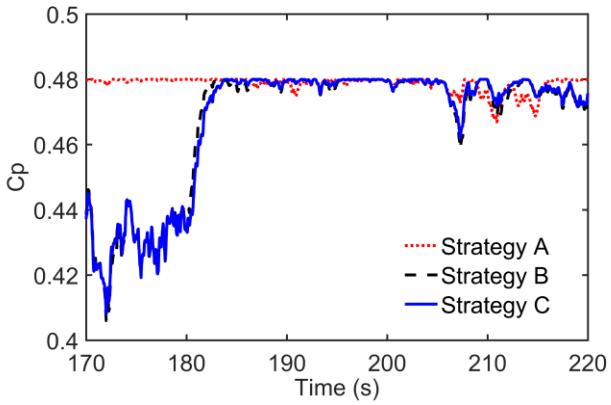

e

Figure. 10 Simulation results of Case. C (170s~220s)

(a) variation of system frequency in Case. C (170s~220s), (b) variation of rotor speed in Case. C (170s~220s), (c) variation of DC-link voltage in Case. C (170s~220s), (d) variation of active power produced by each PMSG-WT in Case. C (170s~220s), (e) variation of power coefficient C_p in Case. C (170s~220s)

Table 11 Frequency performance of Case. C

Schemes	mean value of $\|\Delta f\|$ (Hz) during 100s~180s	f_{nadir} (Hz) during 170s~220s
Strategy A	0.0258	49.6480
Strategy B	0.0214	49.7619
Strategy C	0.0175	49.7681

Table 12 States of each PMSG-WT in Case. C

Schemes	Initial Active Power (p.u.)	Final Active Power (p.u.)	Initial Reactive Power (p.u.)	Final Reactive Power (p.u.)
Strategy A	0.2630	0.3778	0	-0.0173
Strategy B	0.2328	0.3343	0	-0.0090
Strategy C	0.2328	0.3245	0	-0.0079

Table 13 States of 50MVA Thermal Power Plant in Case. C

Schemes	Initial Active Power (p.u.)	Final Active Power (p.u.)	Initial Reactive Power (p.u.)	Final Reactive Power (p.u.)
Strategy A	0.5030	0.5809	0.0530	0.0758
Strategy B	0.5089	0.5907	0.0532	0.0762
Strategy C	0.5089	0.5914	0.0532	0.0756

Table 14 States of 25MVA Thermal Power Plant in Case. C

Schemes	Initial Active Power (p.u.)	Final Active Power (p.u.)	Initial Reactive Power (p.u.)	Final Reactive Power (p.u.)
Strategy A	0.5155	0.5997	0.0512	0.0701
Strategy B	0.5156	0.5942	0.0514	0.0702
Strategy C	0.5157	0.5952	0.0514	0.0696

The simulation results during 170s~220s are shown in Figure. 10 and Table 11. After load increases, the f_{nadir} can be improved greatly if Strategy B or Strategy C is used. By applying Strategy B or Strategy C, the PMSG-WT decelerates and power coefficient approaches to the C_p^{max}, which is 0.48 in this research. The increase of C_p reveals that more wind power can be captured. In addition, the kinetic energy of rotor is also released to the power grid. During this event, the highest value of f_{nadir} can be acquired if Strategy C is applied, because the energy stored in DC capacitor is also utilized for frequency control.

4.4 Sensitivity Analysis of Capacitance Under Case. A

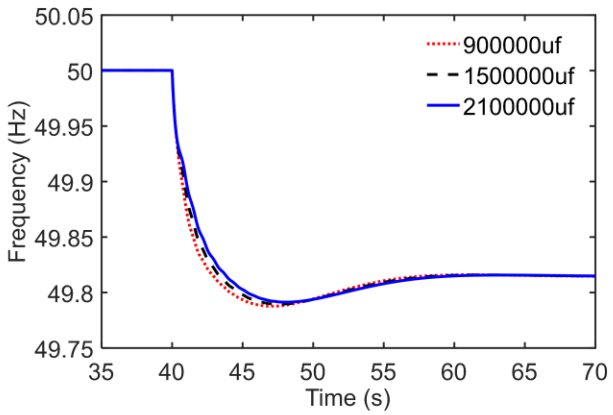

Figure. 11 Frequency performance under different DC capacitance

The sensitivity analysis is conducted by applying the Strategy C with different values of C_{DC}. The simulation results are presented in Figure.11 and Table 15.

Table 15 Data of frequency performance under different DC capacitance

Values of C_{DC} (μf)	Maximum |ROCOF|(Hz/s)	f_{nadir} (Hz)	f_{final} (Hz)
900000	0.2918	49.7877	49.8146
1500000	0.2988	49.7895	49.8146
2100000	0.3021	49.7913	49.8146

From the table, we can learn that the larger C_{DC} leads to greater maximum value of $|ROCOF|$. The reason is that as the C_{DC} becomes larger, the discharge rate of the DC capacitor will become smaller. As a result, the DC capacitor with greater C_{DC} may not be able to provide the frequency support instantaneously after the frequency event is detected and thus the ROCOF may not be suppressed in time. However, more energy can be released if the C_{DC} is larger. Consequently, the highest f_{nadir} can be recorded when C_{DC} is set as 2100000 μf. In addition, the DC capacitor can only provide temporary frequency support. Therefore, the value of f_{final} is not influenced.

5 Conclusion and Discussion

In this paper, we develop a combined control scheme enabling PMSG-WT to

provide primary frequency support. The control scheme consists of rotor speed adjusting control and DC-link voltage regulating control.

Under normal condition, the de-loading operation for primary reserve acquisition is realized by using over-speeding technique. Hence, the additional kinetic energy can be stored. If frequency deviates, the rotor speed adjusting control and DC-link voltage regulating control will work together so that the potential capability of the PMSG-WT can be fully exploited for frequency control. Furthermore, the wind turbine with rotor speed adjusting control can change its rotor speed so that the power captured from wind can be adjusted for frequency regulation. Besides, the kinetic energy stored in the rotor can also be utilized for frequency response as well. Moreover, the DC-link voltage regulating controller employs the energy in DC-capacitor for emulated inertia provision. By using such controller, the frequency dynamic performance can be improved further.

The effectiveness of the proposed control approach is demonstrated by simulation results. Without any additional hardware, a significant improvement in frequency behavior can still be observed due to the implementation of the proposed control scheme.

Several technical issues can be discussed further for future research. If the wind speed is relatively high to activate the pitch angle controller, the frequency response provided by pitch angle control can be investigated. Besides, it would be interesting to study the determination of $DL_{del.N}$ and the selection of relevant parameters such as f_{min}^{WT} in practice. Additionally, as the energy in DC capacitor is used for frequency support, the control scheme for restoring the DC-link voltage may be worth developing. Moreover, the power quality issues should be considered for application.

Reference

[1] F. Wilches-Bernal, J. H. Chow, and J. J. Sanchez-Gasca, "A Fundamental Study of

Applying Wind Turbines for Power System Frequency Control," *IEEE Transactions on Power Systems,* vol. 31, no. 2, pp. 1496-1505, 2016.

[2] R. Pena, J. C. Clare, and G. M. Asher, "A doubly fed induction generator using back-to-back PWM converters supplying an isolated load from a variable speed wind turbine," *IEE Proceedings - Electric Power Applications,* vol. 143, no. 5, pp. 380-387, 1996.

[3] R. G. d. Almeida and J. A. P. Lopes, "Participation of Doubly Fed Induction Wind Generators in System Frequency Regulation," *IEEE Transactions on Power Systems,* vol. 22, no. 3, pp. 944-950, 2007.

[4] D. Ochoa and S. Martinez, "Fast-Frequency Response Provided by DFIG-Wind Turbines and its Impact on the Grid," *IEEE Transactions on Power Systems,* vol. 32, no. 5, pp. 4002-4011, 2017.

[5] K. V. Vidyanandan and N. Senroy, "Primary frequency regulation by deloaded wind turbines using variable droop," *IEEE Transactions on Power Systems,* vol. 28, no. 2, pp. 837-846, 2013.

[6] S. Ghosh, S. Kamalasadan, N. Senroy, and J. Enslin, "Doubly Fed Induction Generator (DFIG)-Based Wind Farm Control Framework for Primary Frequency and Inertial Response Application," *IEEE Transactions on Power Systems,* vol. 31, no. 3, pp. 1861-1871, 2016.

[7] M. F. M. Arani and E. F. El-Saadany, "Implementing Virtual Inertia in DFIG-Based Wind Power Generation," *IEEE Transactions on Power Systems,* vol. 28, no. 2, pp. 1373-1384, 2013.

[8] R. Chen, W. Wu, H. Sun, Y. Hu, and B. Zhang, "Supplemental control for enhancing primary frequency response of DFIG-based wind farm considering security of wind turbines," in *2014 IEEE PES General Meeting | Conference & Exposition*, 2014, pp. 1-5.

[9] J. M. Mauricio, A. Marano, A. Gomez-Exposito, and J. L. M. Ramos, "Frequency Regulation Contribution Through Variable-Speed Wind Energy Conversion Systems," *IEEE Transactions on Power Systems,* vol. 24, no. 1, pp. 173-180, 2009.

[10] F. Díaz-González, M. Hau, A. Sumper, and O. Gomis-Bellmunt, "Participation of wind power plants in system frequency control: Review of grid code requirements and control methods," *Renewable and Sustainable Energy Reviews,* vol. 34, pp. 551-564, 2014/06/01/ 2014.

[11] L. Holdsworth, J. B. Ekanayake, and N. Jenkins, "Power system frequency response from fixed speed and doubly fed induction generator-based wind turbines," *Wind Energy,* vol. 7, no. 1, pp. 21-35, 2004.

[12] Y. Fu, Y. Wang, and X. Zhang, "Integrated wind turbine controller with virtual inertia and primary frequency responses for grid dynamic frequency support," *IET Renewable Power Generation*, vol. 11, no. 8, pp. 1129-1137Available: http://digital-library.theiet.org/content/journals/10.1049/iet-rpg.2016.0465

[13] M. F. M. Arani and Y. A. R. I. Mohamed, "Dynamic Droop Control for Wind Turbines Participating in Primary Frequency Regulation in Microgrids," *IEEE Transactions on Smart Grid,* vol. PP, no. 99, pp. 1-1, 2017.

[14] M. F. M. Arani and Y. A. R. I. Mohamed, "Analysis and Impacts of Implementing Droop Control in DFIG-Based Wind Turbines on Microgrid/Weak-Grid Stability," *IEEE Transactions on Power Systems,* vol. 30, no. 1, pp. 385-396, 2015.

[15] O. Anaya-Lara, F. Hughes, N. Jenkins, and G. Strbac, "Contribution of DFIG-based wind farms to power system short-term frequency regulation," *IEE Proceedings-Generation, Transmission and Distribution,* vol. 153, no. 2, pp. 164-170, 2006.
[16] Y. Wang, J. Meng, X. Zhang, and L. Xu, "Control of PMSG-Based Wind Turbines for System Inertial Response and Power Oscillation Damping," *IEEE Transactions on Sustainable Energy,* vol. 6, no. 2, pp. 565-574, 2015.
[17] N. A. Orlando, M. Liserre, R. A. Mastromauro, and A. Dell'Aquila, "A survey of control issues in PMSG-based small wind-turbine systems," *IEEE transactions on Industrial Informatics,* vol. 9, no. 3, pp. 1211-1221, 2013.
[18] R. Cardenas, R. Peña, S. Alepuz, and G. Asher, "Overview of control systems for the operation of DFIGs in wind energy applications," *IEEE Transactions on Industrial Electronics,* vol. 60, no. 7, pp. 2776-2798, 2013.
[19] N. Freire, J. Estima, and A. Cardoso, "A comparative analysis of PMSG drives based on vector control and direct control techniques for wind turbine applications," *Przegląd Elektrotechniczny,* vol. 88, no. 1, pp. 184-187, 2012.
[20] R. Melício, V. M. F. Mendes, and J. P. d. S. Catalão, "A pitch control malfunction analysis for wind turbines with permanent magnet synchronous generator and full-power converters: proportional integral versus fractional-order controllers," *Electric Power Components and Systems,* vol. 38, no. 4, pp. 387-406, 2010.
[21] M. Seixas, R. Melício, and V. Mendes, "Offshore wind energy system with DC transmission discrete mass: modeling and simulation," *Electric Power Components and Systems,* vol. 44, no. 20, pp. 2271-2284, 2016.
[22] Z. Wu, W. Gao, J. Wang, and S. Gu, "A coordinated primary frequency regulation from Permanent Magnet Synchronous Wind Turbine Generation," in *2012 IEEE Power Electronics and Machines in Wind Applications*, 2012, pp. 1-6.
[23] Z. S. Zhang, Y. Z. Sun, J. Lin, and G. J. Li, "Coordinated frequency regulation by doubly fed induction generator-based wind power plants," *IET Renewable Power Generation,* vol. 6, no. 1, pp. 38-47, 2012.
[24] Y. Li, Z. Xu, and K. P. Wong, "Advanced Control Strategies of PMSG-Based Wind Turbines for System Inertia Support," *IEEE Transactions on Power Systems,* vol. 32, no. 4, pp. 3027-3037, 2017.
[25] J. Licari, J. Ekanayake, and I. Moore, "Inertia response from full-power converter-based permanent magnet wind generators," *Journal of Modern Power Systems and Clean Energy,* journal article vol. 1, no. 1, pp. 26-33, June 01 2013.
[26] S. Heier, "Grid integration of wind energy conversion systems, 1998," *ISBN 0,* vol. 471, p. 97143, 2002.
[27] V. Akhmatov, *Induction generators for wind power*. Multi-Science Pub., 2005.
[28] L. Yang, Z. Xu, J. Ostergaard, Z. Y. Dong, and K. P. Wong, "Advanced Control Strategy of DFIG Wind Turbines for Power System Fault Ride Through," *IEEE Transactions on Power Systems,* vol. 27, no. 2, pp. 713-722, 2012.
[29] Y. Wang, H. Bayem, M. Giralt-Devant, V. Silva, X. Guillaud, and B. Francois, "Methods for Assessing Available Wind Primary Power Reserve," *IEEE Transactions on Sustainable Energy,* vol. 6, no. 1, pp. 272-280, 2015.
[30] A. Buckspan, L. Pao, J. Aho, and P. Fleming, "Stability analysis of a wind turbine active power control system," in *American Control Conference (ACC), 2013*, 2013, pp. 1418-1423: IEEE.

[31] A. Koerber and R. King, "Combined Feedback-Feedforward Control of Wind Turbines Using State-Constrained Model Predictive Control," *IEEE Transactions on Control Systems Technology,* vol. 21, no. 4, pp. 1117-1128, 2013.
[32] J. Zhu, C. D. Booth, G. P. Adam, A. J. Roscoe, and C. G. Bright, "Inertia Emulation Control Strategy for VSC-HVDC Transmission Systems," *IEEE Transactions on Power Systems,* vol. 28, no. 2, pp. 1277-1287, 2013.
[33] X. Wang, X. Ruan, S. Liu, and K. T. Chi, "Full feedforward of grid voltage for grid-connected inverter with LCL filter to suppress current distortion due to grid voltage harmonics," *IEEE Transactions on Power Electronics,* vol. 25, no. 12, pp. 3119-3127, 2010.
[34] S.-A. Amamra, K. Meghriche, A. Cherifi, and B. Francois, "Multilevel Inverter Topology for Renewable Energy Grid Integration," *IEEE Transactions on Industrial Electronics,* vol. 64, no. 11, pp. 8855-8866, 2017.
[35] D. Chen, J. Zhang, and Z. Qian, "An improved repetitive control scheme for grid-connected inverter with frequency-adaptive capability," *IEEE Transactions on Industrial Electronics,* vol. 60, no. 2, pp. 814-823, 2013.
[36] IEEE Commitee Report, "Dynamic Models for Steam and Hydro Turbines in Power System Studies"," *IEEE Transactions on Power Apparatus and Systems,* vol. PAS-92, no. 6, p. 11, 1973.
[37] P. Kundur, N. J. Balu, and M. G. Lauby, *Power system stability and control*. McGraw-hill New York, 1994.
[38] "DTU Database on Wind Characteristics," http://www.winddata.com/, accessed on 10 May 2014.

Appendix

(1) Parameters of the wind turbine:
WT: Rated wind speed is 13.33m/s; inertia constant $H_t = 2.5\text{s}$; damping coefficient $D_{sh} = 1.11\text{p.u.}$; shaft stiffness coefficient $K_{sh} = 1.5\text{p.u.}$; time constant of the pitch servo $T_p = 0.25\text{s}$; $\beta_{max} = 27deg$.

PMSG: Rated power is 2MW; inertia constant $H_g = 0.62\text{s}$; friction coefficient $B = 0.01\text{p.u.}$; stator resistance $R_s = 0.006\text{p.u}$, d-axis synchronous reactance (p.u.): x_d=1.305, x'_d=0.296, x''_d=0.252; q-axis synchronous reactance (p.u.): x_q=0.474, x'_q=0.474, x''_q=0.243, $U_{dc.N} = 2000\text{V}$, $C_{dc} = 1500000\mu f$, $L_g = 0.15p.u.$, $R_g = 0.003p.u.$.

(2) Parameter of excitation system in thermal power plant 1&2:
Regulator gain K_{ES}: 300; time constant T_{ES}: 0.01s.

(3) Parameter of governor in thermal power plant-1:
Servo-motor time constant T_{sm}: 0.025s, gate closing rate $V_{G.MIN}$ -0.1 p.u./s; gate opening rate $V_{G.MAX}$ 0.1 p.u./s; Governor time constants T_2=0s, T_3=0.3s, T_4=4s, T_5=0.1s; Turbine torque fractions F_2=0, F_3=0.3, F_4=0.4, F_5=0.3; droop value R_P=4%.

(4) Parameter of governor in thermal power plant-2:
Servo-motor time constant T_{sm}: 0.025s, gate closing rate $V_{G.MIN}$ -0.1 p.u./s; gate opening rate $V_{G.MAX}$ 0.1 p.u./s; Governor time constants T=0.2s; droop value R_P=4%

(5) Parameter of synchronous generator in thermal power plant-1:

Nominal power 50 MVA; d-axis synchronous reactance: x_d=2.54 p.u., x'_d=0.237 p.u., x''_d=0.183 p.u.; q-axis synchronous reactance x_q=2.31 p.u., x'_q=0.392 p.u., x''_q=0.191 p.u.; inertial contant 5s; friction factor 0.01; stator resistance 0.0021 p.u.

(6) Parameter of synchronous generator in thermal power plant-2:
Nominal power: 25 MVA; d-axis synchronous reactance: x_d=2.349 p.u., x'_d=0.219 p.u., x''_d=0.169 p.u.; q-axis synchronous reactance x_q=2.136 p.u., x'_q=0.362 p.u., x''_q=0.177 p.u.; inertial contant 5s; friction factor 0.01; stator resistance 0.002 p.u.